UCRL-JC-144223

Structural Modification in Fused Silica Due to Laser Damage Induced Shock Compression

A. Kubota, M-J Caturla, L. Davila, J. Stolken,
B. Sadigh, A. Quong, A. Rubenchik and M.D. Feit

This article was submitted to the Boulder Symposium on Laser-Induced Damage in Optical Materials, Boulder, Colorado, October 1-3, 2001

U.S. Department of Energy

Lawrence Livermore National Laboratory

December 5, 2001

Structural modifications in fused silica due to laser damage induced shock compression

Alison Kubota*, Maria-Jose Caturla, Lilian Davila, James Stolken, Babak Sadigh, Andrew Quong, Alexander Rubenchik and Michael D. Feit.

Lawrence Livermore National Laboratory, L-370, Livermore, CA 94551

ABSTRACT

High power laser pulses can produce damage in high quality fused silica optics that can lead to its eventual obscuration and failure. Current models suggest the initiation of a plasma detonation due to absorbing initiators and defects, leading to the formation of shock waves. Recent experiments have found a densified layer at the bottom of damage sites, as evidence of the laser-damage model. We have studied the propagation of shock waves through fused silica using molecular dynamics. These simulations show drastic modifications in the structure and topology of the network, in agreement with experimental observations.

Keywords: Laser-materials interactions; fused silica, shock compression, densification, phase transformation, molecular dynamics simulations, laser damage.

1. INTRODUCTION

The interaction of lasers with materials has been of increased interest over the past several years. There have been many developments in the application of lasers for materials processing. These applications include surface modification and conditioning[1], waveguide fabrication[2], laser peening, ultrafast micromachining[3,4,5] and channel drilling[3,4]. Of increased interest are also the unintentional modifications of lasers to materials, in particular, laser optics. The gradual damage of fused silica optics[6] used in higher wavelength photolithographic patterning has become increasingly problematic as increasing device integration requirements continue to necessitate smaller devices. In the area of inertial fusion energy (IFE) research, recent efforts have been focused on the mitigation of damage initiation and growth in fused silica UV optics[7].

One of the unusual properties of fused silica is its ability to undergo permanent densification under many different modes of damage formation such as under static compression[8], shock compression[9] from flyer plate experiments, neutron irradiation[10] and UV irradiation[6]. In addition, Raman spectroscopy measurements of the damaged fused silica[11] have produced signature D1 and D2 peaks which have been attributed to modifications in the network topology of the material.[12]

Recent efforts have been devoted to the understanding of the damage formation of fused silica due to high-powered laser irradiation. The current understanding of laser-damage[7] involves the coupling of the material to the initial and successive laser pulses through either foreign defects (UV absorbing ceria, metallic particles, etc) or absorbing defects created during a damage event. Associated with the damage event is the formation of a plasma (which further couples with the laser) and a detonation leading to ablation and densification of fused silica. Recent experiments[13] have revealed evidence of this densified layer at the bottom of microcraters produced during laser-damage events.

In this paper, we focus on the atomistic modeling of shockwaves propagating through fused silica. The work presented here is based on previous preliminary calculations[14] performed on shocks. It is believed that the intrinsic characteristics of the densified and defected fused silica are responsible for the further coupling of the UV laser energy to the material.

* Correspondence: Email: kubota1@llnl.gov; Telephone: 925 424 6125; Fax: 925 423 0909

Thus, a detailed understanding of the densification and damage process during and after the shock propagation is vital towards the development of damage mitigation techniques and damage resistant UV materials.

2. MODELING

We have applied Molecular Dynamics (MD) to study the propagation of shocks through fused silica. Molecular dynamics is capable of integrating the motion of an ensemble of particles, provided a potential which fully describes the interactions between all the atoms. The empirical interatomic potential used in this study are those developed by Feuston and Garofalini[15] and have been successfully applied to studies on the densification of silica[16]. This potential includes pairwise and three-body terms to account for the ionic and covalent bonding of the amorphous fused silica network.

Two sizes of computational cells were used for the assurance of negligible supercell-size-effects. For the larger cell, the initial conditions for the simulation were taken as amorphous SiO_2 contained within a 71.6Å x 71.6Å x 716Å computational supercell. This cell, containing a total of 240,000 atoms (80,000 SiO_2 units) was formed through a melt-quench sequence beginning with a β-cristobalite configuration. This sequence involved melting the β-cristobalite at 7000K for 25 psec with periodic boundary conditions in each direction. This was followed by a series of steps where the temperature was reduced at 1000K increments and simulated for 25 psec. After the supercell is equilibrated at 1000K for 25 psec, the temperature is then reduced to 300K and the periodic boundary condition is released in the direction along the "long" direction of the supercell. This cell is then equilibrated for 25 psec. Figure 1 shows the final simulation cell. The smaller cell was taken as a 71.6Å x 71.6Å x 286.4Å with 96,000 atoms. This cell was prepared in the same manner as above.

The bond-angle distribution of this fused silica configuration compares well with those of experiments[17]. The O-Si-O bond-angle-distribution is centered at 109° with a FWHM of 12°. This compares with 109° and 14° from experiments. However, the critical feature that distinguishes different polymorphs of silica is the Si-O-Si bond-angle-distribution. In our fused silica supercell, the peak is found at 158° with FWHM of 32°, compared to between 144° and 156°, and FWHM of 38° from experiments.

Shocks were propagated through the material with the use of a "piston." The atoms in a slab section at one end of the long supercell are selected and forced at a fixed piston velocity, U_p. This same method has been used in other studies to examine shocks through materials[18,19]. Shock simulations with piston velocities between 0.25 and 2.5 km/sec were performed on the IBM SP Blue Pacific Massively Parallel Supercomputer at LLNL. The MDCASK code was used to run the MD simulations, with each simulation using 32 processors.

Because of the small size of the simulation cell, we have only generated the primary shock, without the trailing release wave. However, we did examined the effect of relaxation of one of the shock simulations. For the case of the 2.5 km/sec piston velocity, the configuration of the shocked material was taken and relaxed (equilibrated) at 300K for 120 psec.

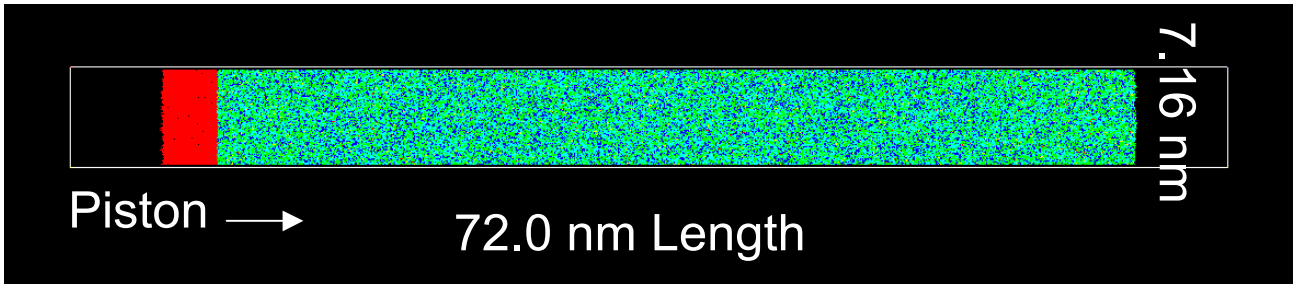

Figure 1: The geometry of the computational cell with 240,000 atoms (80,000 SiO_2 units). The atoms constituting the piston are colored on the left. Shock waves are generated by forcing the piston at constant velocity.

3. RESULTS AND DISCUSSION

Figure 2 shows the calculated shock-velocities compared with experimental data of Sugiura and coworkers[9]. The MD simulations reveal a good agreement with experimental data. In particular, the modeling results follow experiments particularly well not only the transition beyond the elastic limit near 1.0 km/sec piston (particle) velocity, but also the shock velocities in this compressive regime. It is this densification regime which is of most relevance to the issue of laser-driven shock damage in fused silica.

Figure 3 shows the particle velocity distribution of two different shocks generated using pistons driven at 0.75 and 2.0 km/sec. In the case of a 0.75 km/sec shock, which is below the elastic limit, we observe the propagation of a single acoustic wave that traverses the computational cell. The shock, or wave velocities were calculated by averaging over the position of the wavefront from the particle velocity distributions. Below the elastic limit, the wave velocities appear to be overestimated, in comparison to experimental data, as shown in Figure 2. In the case of the 2.0 km/sec shock, well above the elastic limit, we observe the propagation of both the acoustic wave at approximately 7 km/sec followed by the compressive shock wave. The two wavefronts of the particle velocity distributions can be seen clearly in Figure 3.

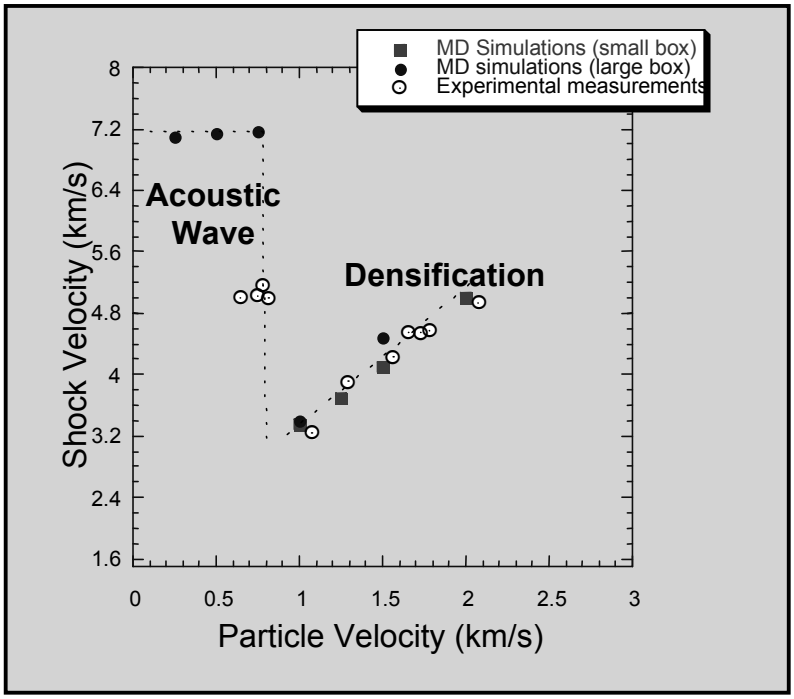

Figure 2: Shock Velocities plotted versus the particle velocities for MD simulations and experimental measurements of Sugiura and coworkers.

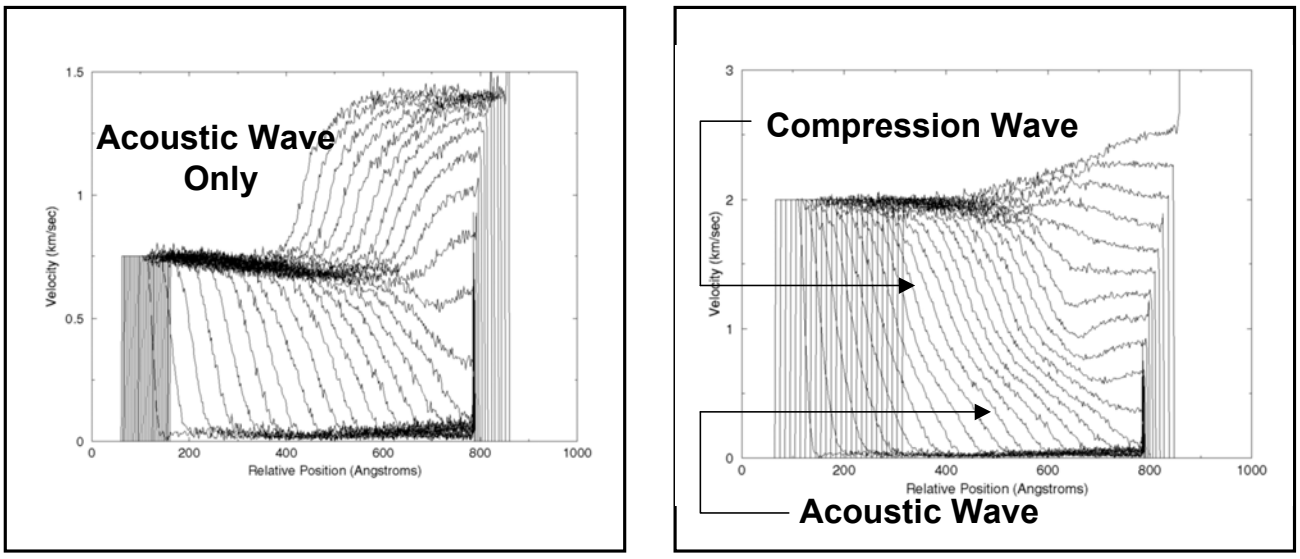

Figure 3: Shock velocity profiles of a 0.75 km/sec and 2.0 km/sec piston, applied from the left. The vertical lines on the left show the position of the piston at 0.5 psec increments. The profile shows the acoustic wave in the lower parts of the profile and ahead of the shock wave. As the acoustic wave reaches the far end of the computational supercell, a release wave is produced back towards the piston.

Detailed analysis was performed on the shock generated with a 2.5 km/sec piston. In this case, the simulation was stopped after the elastic wave reached the end of the computational cell. At this point, the supercell was quenched to 300K and relaxed for 120 psec. Several methods of analysis were performed on (C1) the initial unshocked fused silica, (C2) the configuration of the still compressed fused silica at the end of the shock simulation, and (C3) the configuration of the fused silica after quench and 120 psec relaxation. Understanding the differences in the structures of these three configurations are essential towards understanding the processes of damage and densification during and after shocks.

Coordination analysis was performed on the three configurations. Coordination analysis involves the tabulation of nearest-neighbor Si-O bonds, where a bond is one with an interatomic separation of 2Å. In configuration 1 (C1), or the unshocked fused silica, 99.66% of the Si has coordination 4, while 0.20% and 0.14% have coordinations of 3 and 5, respectively. In general, fused silica and most of the SiO_2 crystalline polymorphs consist of four-fold coordinated Si, with their structures differing by their bond-angle distributions, or more generally, their ring structures.

The C2 configuration represents the fused silica immediately after the shock front has propagated through the silica, and before any relaxation has occurred. Analysis of this configuration gives an indication of the structural modification during the shock. Coordination analysis reveals that up to 4.9% of 5-fold coordinated Si are present, while 1.2% of 3-fold coordinated Si are observed. These changes indicate an enormous disturbance to the material, manifested in terms of the generation of structural defects which are related to changes in the electronic properties. However, after relaxation (C3 configuration), the number of over- and undercoordinated Si is dramatically reduced, though still higher than initially. In addition, densification of 20% was observed comparing the unshocked with the relaxed configurations.

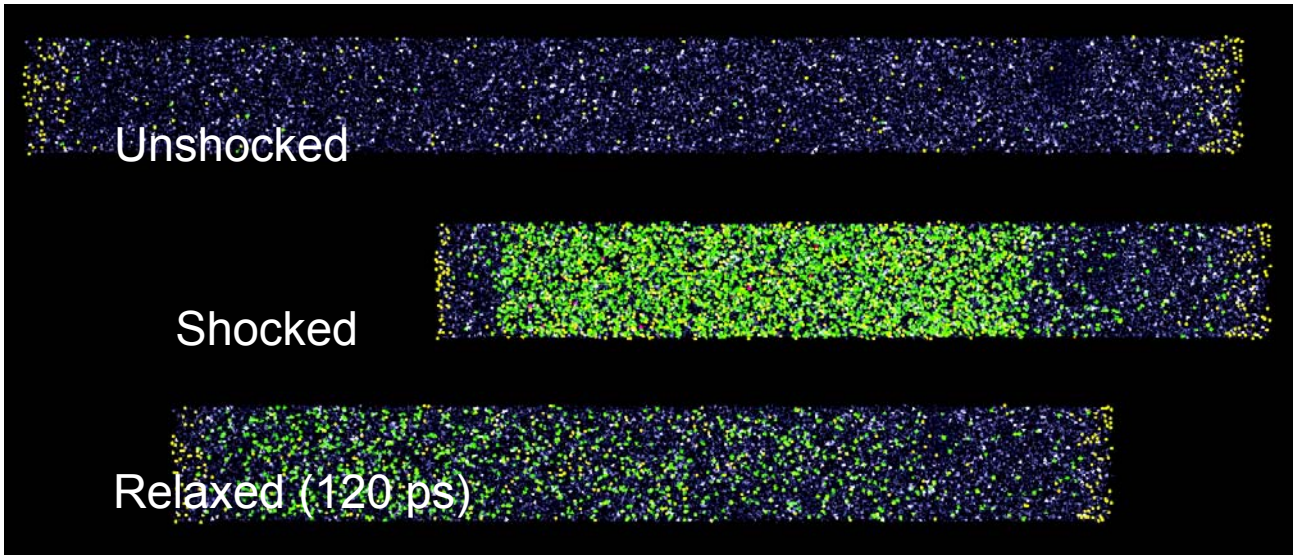

Figure 4: The configurations of the unshocked (C1), shocked (C2) and relaxed (C3) configurations of the fused silica supercell. 3-fold (oxygen deficient centers) and overcoordinated coordinated Si are shown as small bright spots.

The ring distribution defines most generally, the topology of the network glass. Most crystalline silica polymorphs are composed of 6-membered and 8-membered rings. An n-membered ring is defined as the shortest-path circuit covering 2n Si-O bonds. The ring size distribution for the C1 configuration is found to peak at 6, with the total number of rings per silicon found to be 5.93. We observe the ring distributions to span between 2- and 10-membered rings, with larger rings not observed.

During shock propagation through the supercell, topological changes in the network are clearly observed. The full ring distributions of the three different configurations are shown in Figure 5. The 5- and 6-membered rings still appear to be the dominant contributor to the ring distribution after the shock. However, the C2 configuration reveals a marked increase in both the numbers of 3-4 membered rings as well as the number of 7-10 membered rings. Figure 6 reveals the drastic increases in both the smaller and larger rings, from the unshocked to shocked fused silica. There have been many reports emphasizing the significance of the smaller 3- and 4-membered rings. West and Hench[20] have shown that these strained rings have reduced activation barriers to chemical reactions and bond scission. In addition, the D2 and D1 Raman spectra signatures at 606 cm^{-1} and 492 cm^{-1} have been attributed to the breathing modes of the 3- and 4-membered rings, respectively.[12]

Ring analysis of the relaxed C3 configuration show the persistent increase in the 3- and 4-membered rings compared with the unshocked C1 configuration. In addition, the 7-and-larger-membered rings also show persistent increases in their contributions to the ring distribution. These persistent changes in the ring coordination indicate the formation of a stable phase of permanently densified fused silica. The large increases observed in the larger rings also suggest the disruption of the fused silica network, and may indicate the existence of cracks, and microvoids. The increases in the smaller strained rings are a plausible connection to the observed permanent densification. The role of the larger rings upon densification is not clear. However the ability for large rings to exist in compact non-planar configurations suggests that their impact on density is small.

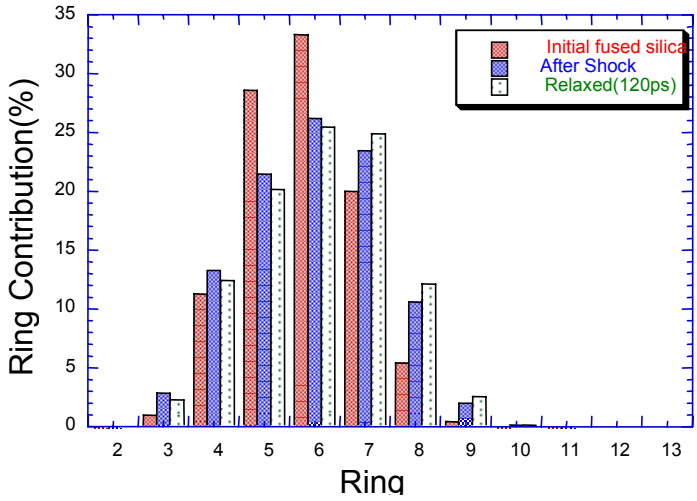

Figure 5: The Ring distibutions of the unshocked (C1), shocked (C2) and relaxed (C3) configurations of fused silica.

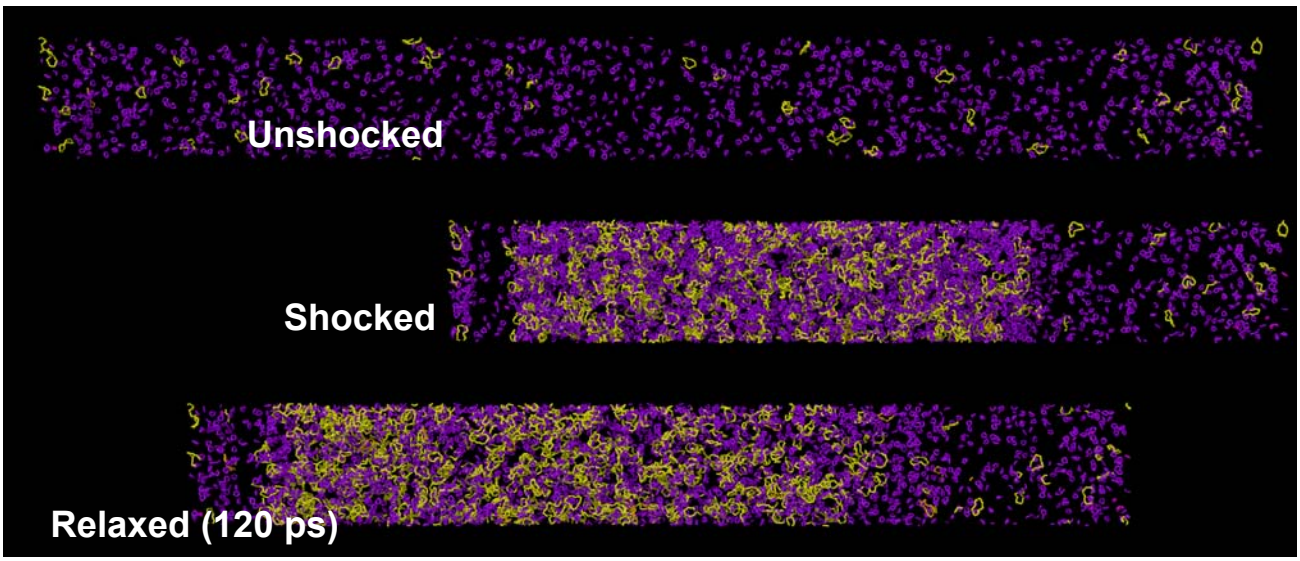

Figure 6: The unshocked (C1), shocked (C2) and relaxed (C3) configurations of fused silica showing only the 2-4 membered rings (dark rings) as well as rings with size 10 and larger (bright rings).

The structure factor S(q) was calculated from the atomic coordinates for the C1 and C3 configurations, and are shown in Figure 7. The first sharp diffraction peak (FSDP) is indicated in Figure 7, and represents order that extends beyond the nearest-neighbor distance. This indication of intermediate-range order, has been observed in static compression experiments of Meade and coworkers[8]. We observe that the FSDP is dramatically suppressed and shifted towards larger q after shock compression and relaxation. This suppression is an indication of significant loss of medium range order due to the shock. Furthermore, this suppression and shift in FSDP has been observed experimentally in static compression experiments of fused silica. Hence, the structural changes in fused silica appear to be similar in both dynamic shock-compression and quasistatic compression.

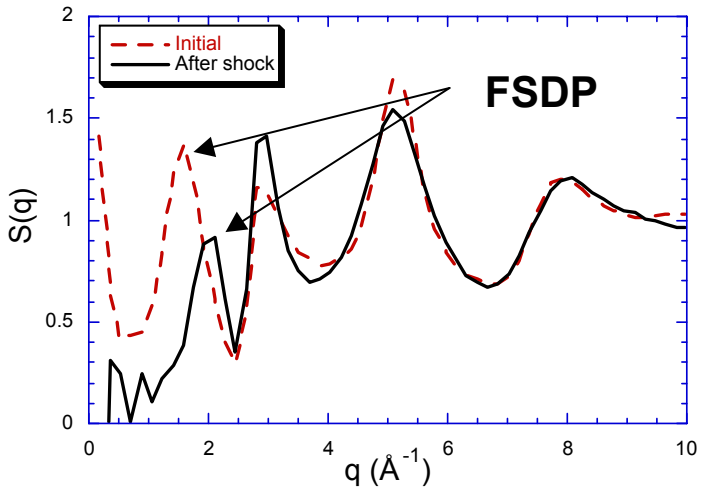

Figure 7: The structure factor S(q) calculated from the atomic positions of the unshocked and shocked fused silica lattices. The first sharp diffraction peak is reduced and shifted to larger q after the shock.

As a further validation of the loss of medium-range-order, we have calculated the pair-correlation function g(r) between the center-of-mass of small rings (smaller than 5-membered) with the center-of-mass of larger rings (larger than 6-membered). The pair correlation functions are shown in Figure 8. In the initial, unshocked fused silica, we observe sharp features at 2Å and 4Å. The presence of these peaks strongly indicates a *correlation between the smaller and larger rings*. This correlation is lost after the shock, and is unrecovered even after relaxation. Thus, we can assert that the medium-range-order is principally associated with the ring structure, or more specifically, with the correlation between individual rings.

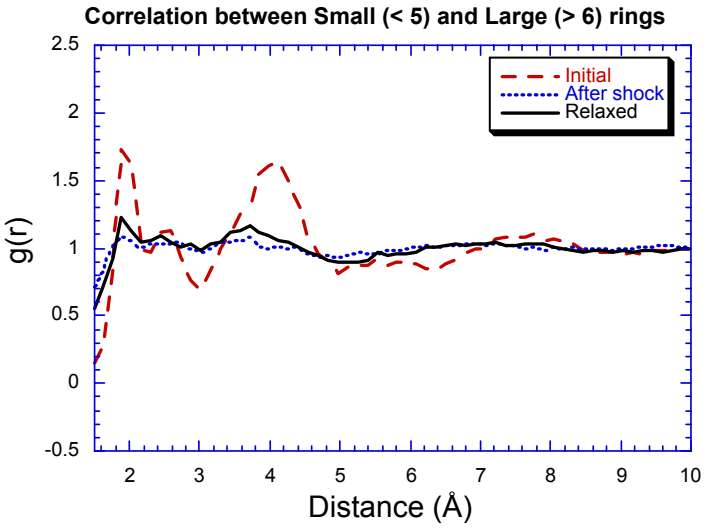

Figure 8: Pair correlation between the family of small (2,3,4-membered) rings with the family of large (7 and larger) rings. Pair correlation of the initial unshocked silica shows peaked features associated with short-ranged and medium-ranged order. Much of the correlation is lost after the shock.

4. CONCLUSIONS

We have used molecular dynamics simulations to understand the atomic-scale structural changes in fused silica due to shock compression. For shock simulations above the Hugoniot Elastic Limit, we observe dramatic changes in the structure and topology of the fused silica network. Densification of approximately 20% was observed for shock simulations with piston velocity of 2.5 km/sec. Similar levels of densification have been observed in laser-damage sites in fused silica, and suggest that similar shock conditions may exist during the laser-damage event. The material modification process during laser damage of fused silica is important for understanding the damage seen during subsequent laser shots.

Coordination analysis of fused silica during the shock reveals a significant increased in under- and overcoordinated Si defects. This observation suggests that there may be strong coupling of the laser to the fused silica during the damage event. In addition, the residual defects remaining after relaxation of the shocked fused silica suggests coupling of the material to subsequent laser shots, thus contributing to the growth of the damage site. This is in-line with the current understanding of laser-damage in fused silica.

We have also observed permanent changes in the network topology of the fused silica. An increase in the number of three- and four-membered rings is observed after the shock, and also after relaxation of the shocked material. This is in agreement with Raman measurements on both flyer-plate compressed and laser-damaged experiments on fused silica. Additionally, increases in 7-and-larger-membered rings is observed both during the shock and after relaxation.

ACKNOWLEDGEMENTS

Special thanks to Stephen Garofalini, Denise Krol, Alan Burnham, Stavros Demos, Joseph Wong, and Thomas Lenosky for their very useful discussions. This work was performed under the auspices of the U.S. Department of Energy by University of California Lawrence Livermore National Labortory under contract No. W-7405-Eng-48.

REFERENCES

1. P. A. Temple, D. Milam and W. Howard Lowdermilk, in Laser Induced Damage in Optical Materials, 229 (1980)
2. D. Krol, Personal Communications (2001)
3. A. Salleo, T. Sands and F. Y. Genin, *Appl. Phys. A*, **71**, 601 (2000)
4. H. Varel, D. Ashkenasi, A. Rosenfeld, M. Wahmer and E. E. B. Campbell, *Appl. Phys. A*. **65**, 367 (1997).
5. J. Jandeleit, P. Ruβbuldt, G. Urbasch, D. Hoffmann, H.-G. Treusch and E. W. Kreutz, *Proc. SPIE*, **3092**, 481.
6. N. F. Borrelli, C. Smith, D. C. Allan and T. P. Seward III*, J. Opt. Soc. Am. B.,* **14**, 1606 (1997).
7. M. D. Feit, L. W. Hrubesh, A. M. Rubenchik and J. Wong, in *Laser-Induced Damage in Optical Materials*, SPIE (In press).
8. C. Meade, R. J. Hemley and H. K. Mao, *Phys. Rev. Lett*. **69**, 1387 (1992).
9. H. Sugiura, R. Ikeda, K. Kondo and T. Yamadaya, *J. Appl. Phys*. **81**, 1951 (1997).
10. W. Primak, and W. Kampwirth, *J. Appl. Phys*. **39**, 5651 (1968)
11. S. G. Demos, L. Sheehan and M. R. Kozlowski, in Laser Applications in *Microelectronic and Optoelectronic Applications V*, Proc. SPIE **3933**, 316 (2000).
12. A. Pasquarello and R. Car, *Phys. Rev. Lett*., **80**, 5145 (1993).
13. J. Wong, D. Haupt, J. H. Kinney, M. Stevens-Kalceft, A. Stesmans, and J. Ferreira, in *Laser-Induced Damage in Optical Materials*, SPIE (in press).
14. A. Kubota, M.-J. Caturla, J. S. Stolken and M. D. Feit, *Optics Express*, **8** (2001).
15. B. P. Feuston and S. H. Garofalini, *J. Chem. Phys*. **89**, 5818 (1999).
16. E. M. Vogel, M. H. Grabow, and S. W. Martin, *J. Non-Crys. Solids*, **204**, 94 (1996).
17. L. Mozzi and B. E. Warren, *J. Appl. Cryst.,* **2**, 164 (1969).
18. A. B. Belonoshko, *Science*, **275**, 955 (1997).
19. D. H. Robertson, J. J. C. Barrett, M. L. Elert and C. T. White., in *Shock Compression of Condensed Matter*, **429**, 297 (1998).
20. J. K. West and L. L. Hench, *J. Am. Ceram. Soc*., **78**, 1093 (1994).